Available online at www.sciencedirect.com
ScienceDirect
Trans. Nonferrous Met. Soc. China 33(2023) 1919−1931
Transactions of Nonferrous Metals Society of China
www.tnmsc.cn

Multiobjective collaborative optimization of novel carbothermal reduction process of stainless steel dust and laterite nickel ore

Pei-jun LIU[1,2,3], Zheng-gen LIU[1,2,3], Man-sheng CHU[4], Rui-jun YAN[1,2,3], Feng LI[1,2,3], Jue TANG[1,2,3]

1. School of Metallurgy, Northeastern University, Shenyang 110819, China;
2. Institute for Frontier Technologies of Low-carbon Steelmaking, Northeastern University, Shenyang 110819, China;
3. Liaoning Province Engineering Research Center for Technologies of Low-Carbon Steelmaking, Northeastern University, Shenyang 110819, China;
4. State Key Laboratory of Rolling and Automation, Northeastern University, Shenyang 110819, China

Received 21 February 2022; accepted 12 August 2022

Abstract: By using the central composite design based on the response surface method, the multiobjective collaborative optimization of Fe, Cr and Ni metal recovery from stainless steel dust and laterite nickel ore was achieved through carbothermal reduction, and a high metal recovery rate and high-grade Fe−Cr−Ni−C alloy particles were obtained. The addition of laterite nickel ore and reduction temperature exert significant effects on the metal recovery, and a significant interaction is observed among the recoveries of the metals Fe, Cr and Ni in the reduction products. The optimal process parameters obtained through the optimization of the model are listed as follows: the amount of added laterite nickel ore is 5.47%, the reduction temperature is 1428.02 °C, the reduction time is 23.10 min, and the carbon oxygen ratio (FC/O) is 0.85. The predicted results for Fe, Cr and Ni recovery using the model are 93.15%, 91.63% and 92.70%, respectively.
Key words: stainless steel dust; laterite nickel ore; metal recycling; response surface methodology; Fe−Cr−Ni−C alloy particles

1 Introduction

The iron and steel industry is an industry with a high level of energy consumption world-wide [1−4]. According to statistics, in 2020, China's stainless steel output reached 30.14 million tons, and the amount of stainless steel dust generated in the smelting process reached 0.9 million tons [5,6]. Stainless steel dust contains a large number of oxides of the valuable metals Fe, Cr and Ni, especially Ni, which has a high price. The recovery of Ni is very important [7,8]. Recycling stainless steel dust from iron-containing solid waste through a reasonable process flow may reduce the waste of the secondary resources and alleviate resource consumption [9].

Pyrometallurgy is the most widely used method in the recycling of iron containing solid waste [10−13]. PENG et al [14] performed the direct reduction of carbon containing stainless steel dust particles and achieved a reduction recovery of Ni and Fe more than 90%, along with a reduction recovery of Cr less than 80%. TANG et al [15] carried out the thermal reduction experiment of mixing and compacting iron containing dust and coal into pellets at high temperature. The results show that the basicity of slag is greater than 1.80, and the reduction products can be separated naturally. The Fe recovery of the product was more than 95% at the reduction temperature above 1350 °C. At present, the methods for treating iron-

Corresponding author: Zheng-gen LIU, Tel: +86-24-83684959, E-mail: liuzg@smm.neu.edu.cn;
Man-sheng CHU, Tel: +86-24-83684959, E-mail: chums@smm.neu.edu.cn
DOI: 10.1016/S1003-6326(23)66232-6

containing solid waste are generally faced with the problems of a high smelting energy consumption, low metal recovery and high basicity. Therefore, adding raw materials with low basicity to solve the high basicity problem of stainless steel dust is an approach to improve the metal recovery from solid waste [16−18]. Laterite nickel ore is a raw material used for ferronickel alloy smelting with low basicity [19,20]. SHIAU [21] studied the suitable carbothermal reduction parameters of low-grade laterite graphite pellets and the effect of the calcination temperature on the carbothermal reduction parameters. The carbon oxygen ratio (FC/O) in laterite nickel ore is 0.6, the reduction temperature is 1100 °C, the reduction time is 30 min, and the Ni grade and Ni recovery of laterite graphite pellets roasted at 400 °C were increased by 30% and 90.2%, respectively. YUAN et al [22] proposed a deep reduction magnetic separation process to enrich Ni and Fe from laterite nickel ore. A nickel iron concentrate with a Ni grade of 6.96%, Ni recovery of 94.06%, Fe grade of 34.74% and Fe recovery of 80.44% was obtained after reduction at a temperature of 1275 °C using a reduction time of 50 min, slag basicity of 1.0, FC/O of 2.5 and magnetic separation of iron concentrate.

The aforementioned research results show that the single factor method is generally used to study the effect of each factor on a single investigated index in studies of Fe-containing solid waste recovery and laterite nickel ore smelting. This study creatively proposed the preparation of carbon-containing briquettes with stainless steel dust, laterite nickel ore and reduction coal (CBSL). The multiobjective collaborative optimization of the recovery of the metals Fe, Cr and Ni was achieved by carbothermal reduction and response surface methodology (RSM). Multiple parameters and interactions were analyzed by RSM using a statistically based optimization strategy [23−27]. By setting the amount of added laterite nickel ore, reduction temperature, reduction time and FC/O ratio as independent variables, the interaction among the metals Fe, Cr and Ni recovery is clarified, the model predicting Fe, Cr and Ni recovery is established, and the best reduction preparation process parameters to achieve high recovery of the metals Fe, Cr and Ni from stainless steel dust and laterite nickel ore are obtained. The obtained Fe−Cr−Ni−C alloy particles can be used as a raw material for steelmaking and promote the sustainable development of iron and steel enterprises.

2 Experimental

2.1 Materials

The raw materials include stainless steel dust, laterite nickel ore and reduction coal. The main components of the stainless steel dust, laterite nickel ore and reduction coal are shown in Tables 1−3. The X-ray diffraction (XRD) analyses of stainless steel dust and laterite nickel ore are shown in Fig. 1.

2.2 CBSL preparation and experimental procedure

Figure 2(a) shows the process used to prepare CBSL. The experimental materials were dried at 110 °C for 6 h in a ventilated drying oven and then crushed and screened through a 200 mesh sieve

Table 1 Chemical composition of stainless steel dust (wt.%)

TFe	FeO	Cr	Ni	CaO	SiO_2	MgO	Al_2O_3	Zn	Loss on ignition
33.18	18.67	11.81	2.10	15.01	4.15	2.87	1.13	0.28	6.48

Table 2 Chemical composition of laterite nickel ore (wt.%)

TFe	FeO	Ni	Cr_2O_3	CaO	SiO_2	MgO	Al_2O_3	P	S	Loss on ignition
19.57	0.21	1.82	1.40	0.09	34.78	12.98	4.00	0.003	0.028	13.02

Table 3 Industrial analysis and ash analysis of reduction coal (wt.%)

FC	Vad	Aad	Mad	Vad analysis					
				CaO	SiO_2	MgO	Al_2O_3	Fe_2O_3	Others
60.58	10.20	28.47	0.75	10.33	40.82	2.92	30.87	5.89	9.17

FC: Fixed carbon content; Vad: Volatilematter content on dry ash free basis; Aad: Ash content on air dry basis; Mad: Moisture on air dry basis

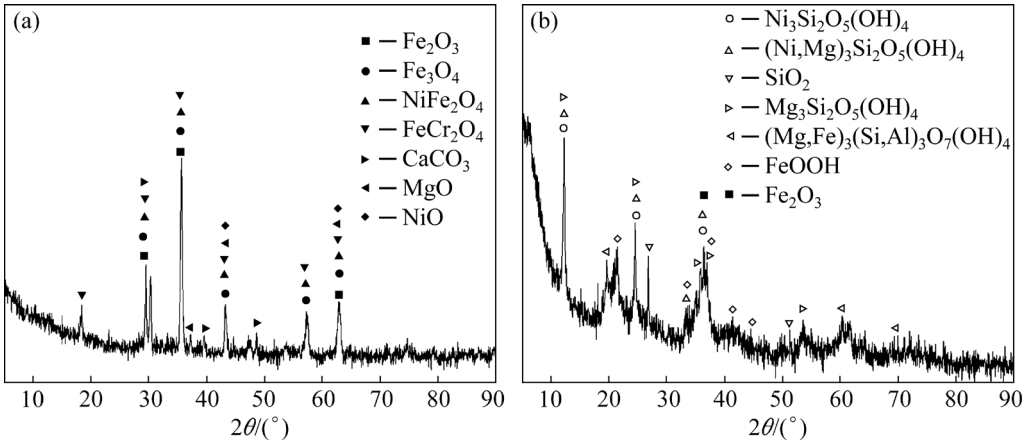

Fig. 1 XRD patterns of stainless steel dust (a) and laterite nickel ore (b)

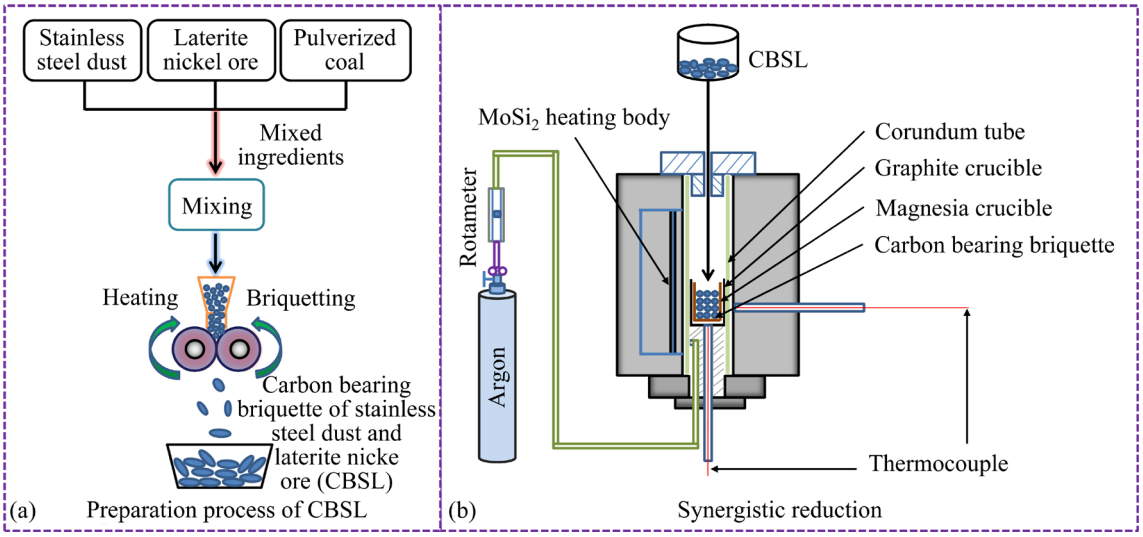

Fig. 2 Process flow charts of CBSL preparation (a) and synergistic reduction natural cooling separation experiment (b)

(particle size less than 74 μm). Finally, elliptical column CBSL composite briquettes were formed by mixing and pressing materials in a certain proportion. FC/O is the molar ratio of fixed carbon in CBSL composite briquettes to oxygen in Fe, Cr and Ni metal oxides [28].

Figure 2(b) shows a schematic diagram of the CBSL carbothermal synergistic reduction experiment. The experimental equipment is a vertical tube high-temperature furnace with a maximum heat-resistant temperature of 1600 °C. The heating element is $MoSi_2$. The temperature measuring element is a thermocouple, and the temperature measurement error is less than 1 °C. In the reduction experiment, the argon flow rate in the corundum tube of the high-temperature furnace was 1.3×10^{-5} m^3/s to maintain an inert atmosphere. After reaching the target temperature, high-temperature refractory gloves and high-temperature experimental clothes were worn. A long handle clamp was used to place the crucible containing the CBSL composite briquette in the high-temperature reduction area of the high-temperature furnace. After reaching the reduction time, the same protective equipment was worn, the same long-handle clamp was used to remove the crucible containing CBSL, and then it was quickly placed into the cooling tank and cooled to room temperature. The cooling tank was filled with argon at a flow rate of 10 L/min to achieve rapid cooling and prevent oxidation. After cooling, the reduction products were removed, and the experiment was completed.

2.3 Experimental index

The recovery of the metals Fe, Cr and Ni from the synergistic reduction products of stainless steel dust and laterite nickel ore is the key parameter investigated and optimization index for the

response surface method. The following equation was used to calculate the metal recovery:

$$R_i = \frac{m_i}{M_i} \times 100\% \quad (1)$$

where R_i is the Fe, Cr and Ni metal recovery rate, m_i is the mass of metal in the reduction product, and M_i is the mass of metal in the raw material.

2.4 Detection and analysis method

The response values in this study are the recovery of Fe, Cr and Ni metals in the reduction product. The enrichment of Fe, Cr and Ni in the reduction products was measured by chemical titration at a professional research institute (Analysis and Testing Center of Northeastern University, China). The phases of raw materials and reduction slag were analyzed using an X-ray diffractometer (MPDDY2094, PANalytical B.V., Almelo, Netherlands). Copper K_α radiation (40 kV, 40 mA, wavelength 0.154 nm) was used as the X-ray source with a scanning angle ranging from 5° to 90° and a scanning speed of 0.2 (°)/s.

2.5 RSM experimental design

Central composite design (CCD) based on RSM is the most commonly used method in experimental design [29−31]. RSM and CCD were used to study the interaction and optimize the variables with the least number of experiments [32−36]. The validity of the equation was analyzed using analysis of variance (ANOVA), and the fitting quality of the equation is judged by calculating the correlation coefficient and P value [37−39]. The second-order polynomial regression model was established through RSM, and the following formula was used for the calculation:

$$Y = \beta_0 + \sum_{i=1}^{k} \beta_i x_i + \sum_{i=1}^{k} \beta_{ii} x_i^2 + \sum_{i=1}^{k-1} \sum_{j=i+1}^{k} \beta_{ij} x_i x_j + \varepsilon \quad (2)$$

where Y is the predicted response, x_i and x_j are the input variables, β_0 is the intercept term, β_i is the linear effect, β_{ii} is the squared effect, β_{ij} is the interaction term, k is the number of factors, and ε is the random error.

Four variables and five levels of CCD were used for the experimental design to investigate the effects of laterite nickel ore addition, reduction temperature, reduction time and FC/O on the Fe recovery, Cr recovery and Ni recovery from CBSL reduction products. The levels of the four independent variables were selected based on previous research. Table 4 lists the five levels of the four variables.

3 Results and discussion

3.1 RSM results

The experimental design matrix obtained using Design Expert is shown in Table 5. The indices in the experiment were obtained through the experiment, and the results are listed in Table 5. Table 5 shows that the recovery rate of Ni metal is always higher than that of Fe metal and Cr metal, indicating that carbothermal reduction achieves the efficient recovery of Ni metal.

With the change in the proportion of stainless steel dust and laterite nickel ore in CBSL, the slag composition and basicity of CBSL changed significantly. The change in basicity exerted a direct effect on the separation of reduction products. The raw material calculation showed that the basicity of the CBSL slag system ranged from 1.65 to 2.78 under the conditions of different amounts of added laterite nickel ore. The amounts of added laterite nickel ore were 0.95%, 11.05% and 6%, and the theoretical basicity of the slag system was 2.78, 1.65 and 2.08, respectively.

3.2 Fitting prediction model

The linear model, two-factor interaction model (2FI), and quadratic model were used to conduct regression fitting of the experimental data in Table 5. The results are presented in Table 6.

Table 4 Values and levels of independent variables used in CCD

Independent variable	Symbol	Range and level				
		−1.68179	−1	0	1	1.68179
Laterite nickel ore addition/%	x_1	0.95	3.00	6.00	9.00	11.05
Reduction temperature/°C	x_2	1315.91	1350.00	1400.00	1450.00	1484.09
Reduction time/min	x_3	11.59	15.00	20.00	25.00	28.41
FC/O	x_4	0.60	0.70	0.85	1.00	1.10

Table 5 Experimental design tests and response results

No.	Variable				Response		
	Laterite nickel ore addition (x_1)/%	Reduction temperature (x_2)/°C	Reduction time (x_3)/min	FC/O (x_4)	Fe recovery rate (Y_1)/%	Cr recovery rate (Y_2)/%	Ni recovery rate (Y_3)/%
1	3.00	1350.00	15.00	0.70	54.63	53.18	59.96
2	9.00	1350.00	15.00	0.70	53.28	52.69	57.43
3	3.00	1450.00	15.00	0.70	71.56	68.41	69.12
4	9.00	1450.00	15.00	0.70	69.53	65.44	67.26
5	3.00	1350.00	25.00	0.70	62.31	59.77	63.36
6	9.00	1350.00	25.00	0.70	60.56	57.48	61.92
7	3.00	1450.00	25.00	0.70	76.64	74.35	79.86
8	9.00	1450.00	25.00	0.70	74.43	73.56	76.28
9	3.00	1350.00	15.00	1.00	55.74	51.22	57.65
10	9.00	1350.00	15.00	1.00	54.27	50.63	55.46
11	3.00	1450.00	15.00	1.00	68.49	67.37	70.42
12	9.00	1450.00	15.00	1.00	66.94	64.16	68.63
13	3.00	1350.00	25.00	1.00	61.18	57.49	62.61
14	9.00	1350.00	25.00	1.00	59.74	56.32	61.07
15	3.00	1450.00	25.00	1.00	75.83	72.23	76.65
16	9.00	1450.00	25.00	1.00	72.65	70.08	74.47
17	0.95	1400.00	20.00	0.85	83.57	81.72	84.33
18	11.05	1400.00	20.00	0.85	75.71	71.62	76.15
19	6.00	1315.91	20.00	0.85	51.73	43.18	53.96
20	6.00	1484.09	20.00	0.85	90.42	88.67	89.86
21	6.00	1400.00	11.59	0.85	74.36	69.85	75.63
22	6.00	1400.00	28.41	0.85	91.24	90.33	92.16
23	6.00	1400.00	20.00	0.60	64.61	60.56	67.41
24	6.00	1400.00	20.00	1.10	69.53	65.17	69.44
25	6.00	1400.00	20.00	0.85	89.51	87.42	88.79
26	6.00	1400.00	20.00	0.85	88.67	86.74	88.35
27	6.00	1400.00	20.00	0.85	89.23	87.37	88.42
28	6.00	1400.00	20.00	0.85	89.07	88.16	87.49
29	6.00	1400.00	20.00	0.85	87.96	87.67	86.89
30	6.00	1400.00	20.00	0.85	89.15	87.06	88.23

Table 6 Statistics summary of simulated results

Source	Fe recovery rate/%			Cr recovery rate/%			Ni recovery rate/%		
	Standard deviation	R^2	Adjusted R^2	Standard deviation	R^2	Adjusted R^2	Standard deviation	R^2	Adjusted R^2
Linear	11.07	0.37	0.27	11.80	0.38	0.28	10.13	0.38	0.28
2FI	12.68	0.37	0.04	13.53	0.38	0.05	11.58	0.38	0.06
Quadratic	3.52	0.96	0.93	4.23	0.95	0.91	3.45	0.96	0.92

As shown in Table 6, among the fitting results for the three simulation statistical models, the regression fitting result from the quadratic model was the best for the experimental data for Fe, Cr and Ni recovery, and the R^2 and adjusted R^2 values from the quadratic model were the largest among the three models, indicating the highest accuracy of the fitting model. The R^2 values of the quadratic models for Fe, Cr and Ni recovery were 0.96, 0.95 and 0.96, respectively, and the adjusted R^2 values of the quadratic models for Fe, Cr and Ni recovery were 0.93, 0.91 and 0.92, respectively. A high correlation was observed between the actual and predicted value. The second-order quadratic model for Fe, Cr and Ni recovery from CBSL reduction products was established as

For Fe recovery:

$$\begin{aligned}Y_1 = &-6490.32 + 7.44x_1 + 8.62x_2 + 7.17x_3 + \\ &772.00x_4 - 1.23\times10^{-3}x_1x_2 - 9.08\times10^{-3}x_1x_3 - \\ &0.04\times x_1x_4 - 7.10\times10^{-4}x_2x_3 - 0.07x_2x_4 - \\ &0.08x_3x_4 - 0.49x_1^2 - 2.99\times10^{-3}x_2^2 - \\ &0.13x_3^2 - 395.33x_4^2 \end{aligned} \quad (3)$$

For Cr recovery:

$$\begin{aligned}Y_2 = &-7029.88 + 8.14x_1 + 9.43x_2 + 5.61x_3 + \\ &713.64x_4 - 1.91\times10^{-3}x_1x_2 + 3.58\times10^{-3}x_1x_3 - \\ &0.08\times x_1x_4 + 3.75\times10^{-4}x_2x_3 - 3.83\times10^{-3}x_2x_4 - \\ &0.23x_3x_4 - 0.50x_1^2 - 3.30\times10^{-3}x_2^2 - \\ &0.13x_3^2 - 415.08x_4^2 \end{aligned} \quad (4)$$

For Ni recovery:

$$\begin{aligned}Y_3 = &-5763.48 + 5.65x_1 + 7.82x_2 + 0.70x_3 + \\ &580.32x_4 - 7.13\times10^{-4}x_1x_2 - 1.54\times10^{-3}x_1x_3 + \\ &0.24\times x_1x_4 + 3.34\times10^{-3}x_2x_3 + 0.03x_2x_4 - \\ &0.42x_3x_4 - 0.44x_1^2 - 2.77\times10^{-3}x_2^2 - \\ &0.11x_3^2 - 362.39x_4^2 \end{aligned} \quad (5)$$

where Y_1, Y_2, and Y_3 are the Fe, Cr and Ni recovery of CBSL reduction products, respectively, and x_1, x_2 and x_3 are the amount of laterite nickel ore added, reduction temperature, and reduction time, respectively.

3.3 ANOVA of response surface

The significance of each item in the model was mainly tested by calculating the P value and F value. P value <0.01 indicates that the item in the model exerts an extremely significant effect. P value <0.01 is obtained for the three designed models of Fe, Cr and Ni recovery, and the lack of fit is 0.0001, <0.0001 and 0.0005, respectively, indicating that the selected quadratic model has a high fitting accuracy and no obvious relative pure error.

In the linear term, x_2 and x_3 exert very significant effects on the recovery of the Fe, Cr and Ni metals, and in the quadratic term, x_1^2, x_2^2, x_3^2 and x_4^2 have a very significant effect. The order of the effect of the reduction parameters on the recovery of the metals Fe, Cr and Ni in CBSL reduction products is reduction temperature > reduction time > amount of laterite nickel ore added > FC/O.

3.4 Evaluation of fitting model

Figures 3(a, b, c) show the residual normal probability distributions of the Fe, Cr and Ni recovery models, respectively. The fits of the three models are extremely good, and the distribution of scattering points is approximately linear, suggesting that the error follows a normal distribution.

Figure 4 shows the comparison between the predicted and actual values of the Fe, Cr and Ni recovery models. The actual and the predicted values also show a high degree of fit, and the scattering of the actual and the predicted values are approximately distributed along a straight line. Based on the analysis described above, the models predicting Fe, Cr and Ni recovery established using RSM are reliable.

3.5 Effect of reduction condition on Fe, Cr and Ni recovery

For a reduction time of 20 min and FC/O of 0.85, the interactive effect of laterite nickel ore addition and reduction temperature on the Fe recovery from CBSL reduction products is shown in Fig. 5(a). As the amount of added laterite nickel ore increases from 3% to 9%, the recovery of metal Fe increases first and then decreases. With the increase in the amount of added laterite nickel ore, the overall basicity of CBSL decreases, and the recovery rate of the metal Fe increases. Stainless steel dust has high basicity, which makes it difficult to separate slag and metal at the reduction end point, resulting in a low recovery. The addition of laterite

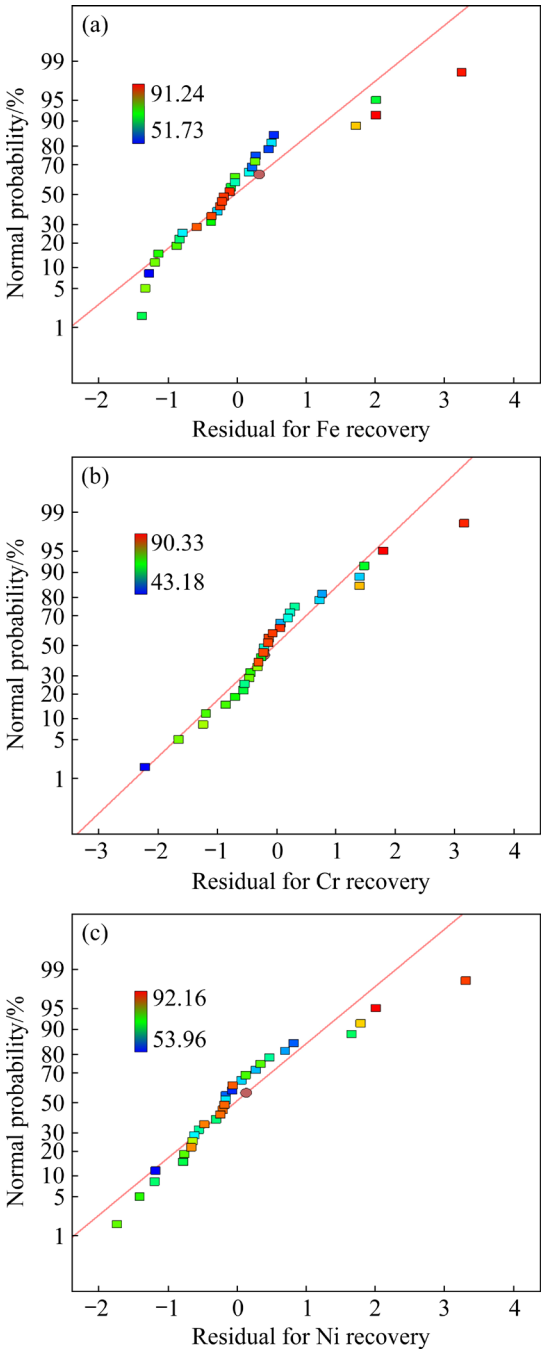

Fig. 3 Normal probability distribution of residuals: (a) Fe recovery; (b) Cr recovery; (c) Ni recovery

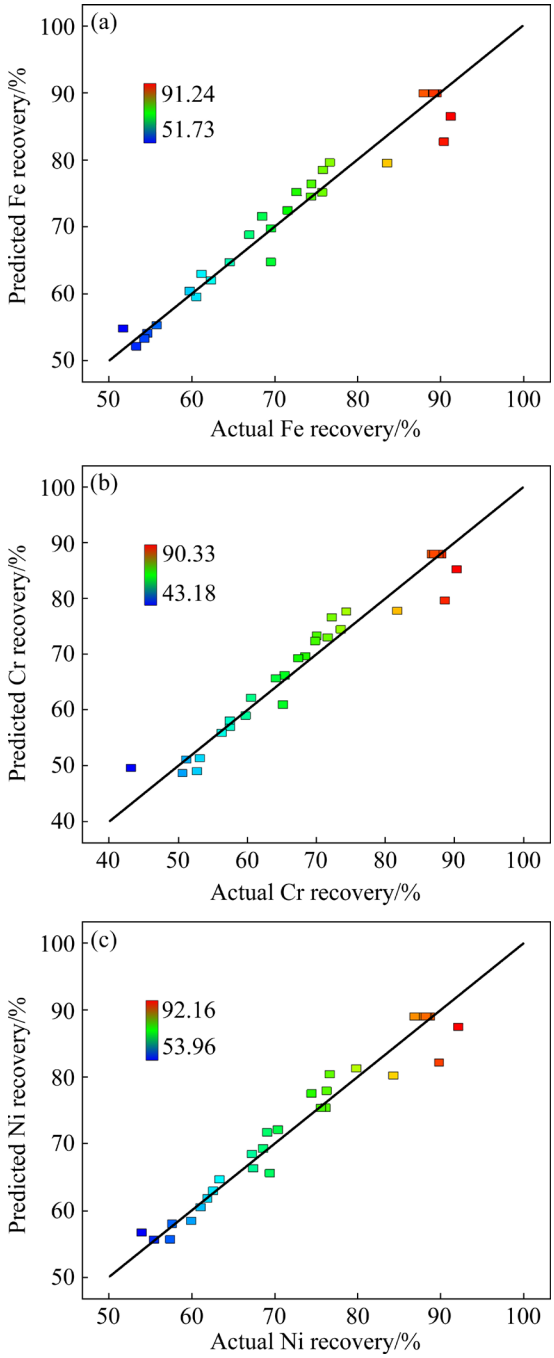

Fig. 4 Comparison between predicted and actual recovery: (a) Fe recovery; (b) Cr recovery; (c) Ni recovery

nickel ore might adjust the overall basicity of CBSL and improve the separation effect of slag and metal to provide good conditions for the aggregation and growth of metal in the reduction process and improve the rate of metal recovered. Low basicity leads to the production of a large number of low-melting point compounds in the reduction products, which hinders the reduction of metal oxides and results in the gradual reduction of metal recovery under certain basicity conditions.

As the reduction temperature increases from 1350 to 1450 °C, the recovery of Fe gradually increases first and then tends to plateau. The increase in reduction temperature is conducive to the reduction of metal. When the reduction temperature exceeds 1400 °C, the recovery rate increases, indicating that when the reduction temperature is 1400 °C, most metal oxides in stainless steel dust reach the reduction limit in the presence of a sufficient reducing agent and a

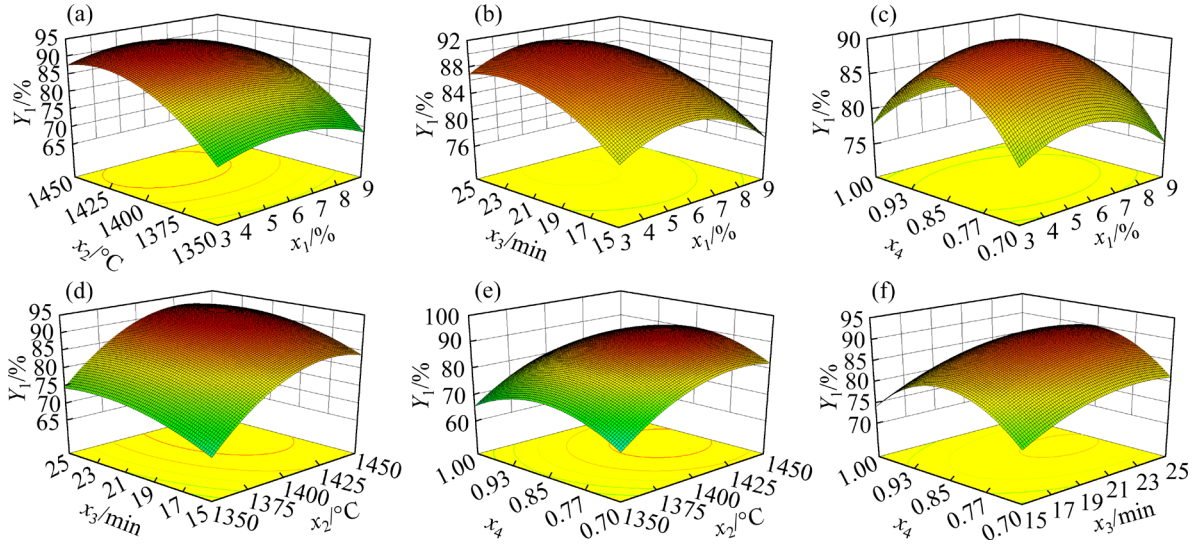

Fig. 5 3D response surface of effects of laterite nickel ore addition (x_1), reduction temperature (x_2), reduction time (x_3), and FC/O (x_4) on Fe recovery (Y_1)

suitable reduction time, and gradually achieve metal reduction. Additionally, the steepness of the reduction temperature direction is greater in Fig. 5(a) than the response surface.

For a reduction temperature of 1400 °C and FC/O of 0.85, the interactive effect of laterite nickel ore addition and reduction time on the Fe recovery in CBSL reduction products is shown in Fig. 5(b). Similar to the effect of reduction temperature on Fe recovery, the Fe recovery initially increases slowly and then plateaus with the extension of the reduction time. Based on these results, prolonging the reduction time is conducive to the reduction of the metal Fe in metal oxides in stainless steel dust. With the extension of the reduction time, the reduction reaction of metal oxides gradually proceeds and ends, which improves the recovery of the metal Fe in CBSL reduction products. After the reduction time reaches 25 min, a high level of recovery of the metal Fe is observed. Compared with the effect of laterite nickel ore addition, the effect of reduction time on Fe recovery is more significant.

Figure 5(c) shows the interactive effect of laterite nickel ore addition and FC/O on the Fe recovery of CBSL reduction products at a reduction temperature of 1400 °C and a reduction time of 20 min. The slope of the response surface changes obviously, and the interaction between laterite nickel ore addition and FC/O on Fe recovery is significant. The FC/O and the laterite nickel ore addition first increase and then decrease metal recovery, suggesting that the content of the reducing agent alters the degree of Fe reduction, and the addition of laterite nickel ore affects the basicity characteristics of raw materials and subsequently affects the recovery rate of the metal Fe. The direction of the effect of laterite nickel ore addition is steeper, and the effect of FC/O is more significant than that of laterite nickel ore addition.

For a system containing 6% laterite nickel ore and an FC/O of 0.85, the interactive effect of reduction temperature and reduction time on the Fe recovery in CBSL reduction products is shown in Fig. 5(d). The slope of the response surface changes obviously, and the interaction between reduction temperature and reduction time on Fe recovery is significant. The direction of the reduction temperature is steeper, and the effect of the reduction temperature is more significant than that of the reduction time.

Figure 5(e) shows the interactive effect of reduction temperature and FC/O on the Fe recovery in CBSL reduction products in the presence of 6% laterite nickel ore and a reduction time of 20 min. The slope of the response surface changes noticeably, and the interaction effect between reduction temperature and FC/O on Fe recovery is significant. The direction of the effect of the reduction temperature is steeper, and the effect of the reduction temperature is more significant than that of FC/O.

The interactive effect of reduction time and FC/O on the Fe recovery of CBSL reduction

products is shown in Fig. 5(f) for a system with 6% laterite nickel ore and a reduction temperature of 1400 °C. The slope of the response surface changes substantially, and the interaction between reduction time and FC/O on Fe recovery is significant. The direction of effect of the reduction time is steeper, and the effect of the reduction time is more significant than that of FC/O.

The interactive effects of various reduction conditions on the Cr and Ni recovery of CBSL reduction products are shown in Figs. 6 and 7, respectively. The interaction of various factors on the Cr and Ni recovery of CBSL reduction products is basically the same as that of Fe recovery, which shows that the interaction of reduction conditions on the recovery of Fe, Cr and Ni is consistent.

3.6 Optimization results and experimental analysis

In the CBSL reduction process, three objective functions (Y_1 of Fe recovery, Y_2 of Cr recovery, and Y_3 of Ni recovery) were considered to optimize the multiobjective expected function. The specific optimization constraints are shown in Table 7.

The final optimal parameters are as follows: amount of added laterite nickel ore of 5.47%, reduction temperature of 1428.02 °C, and reduction time of 23.10 min. Under the optimized conditions,

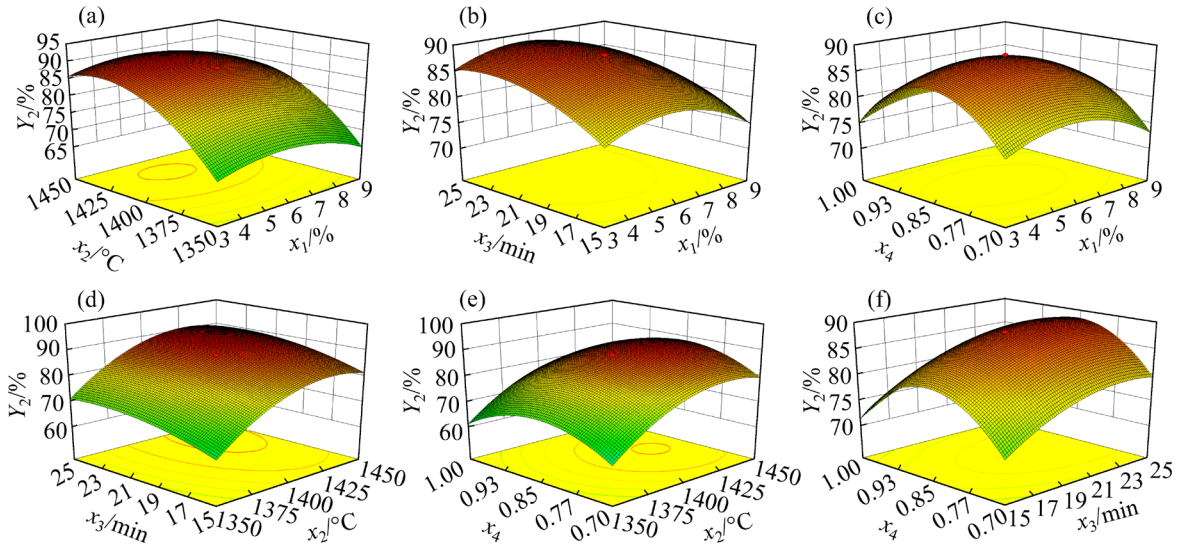

Fig. 6 3D response surface of effects of laterite nickel ore addition (x_1), reduction temperature (x_2), reduction time (x_3), and FC/O (x_4) on Cr recovery (Y_2)

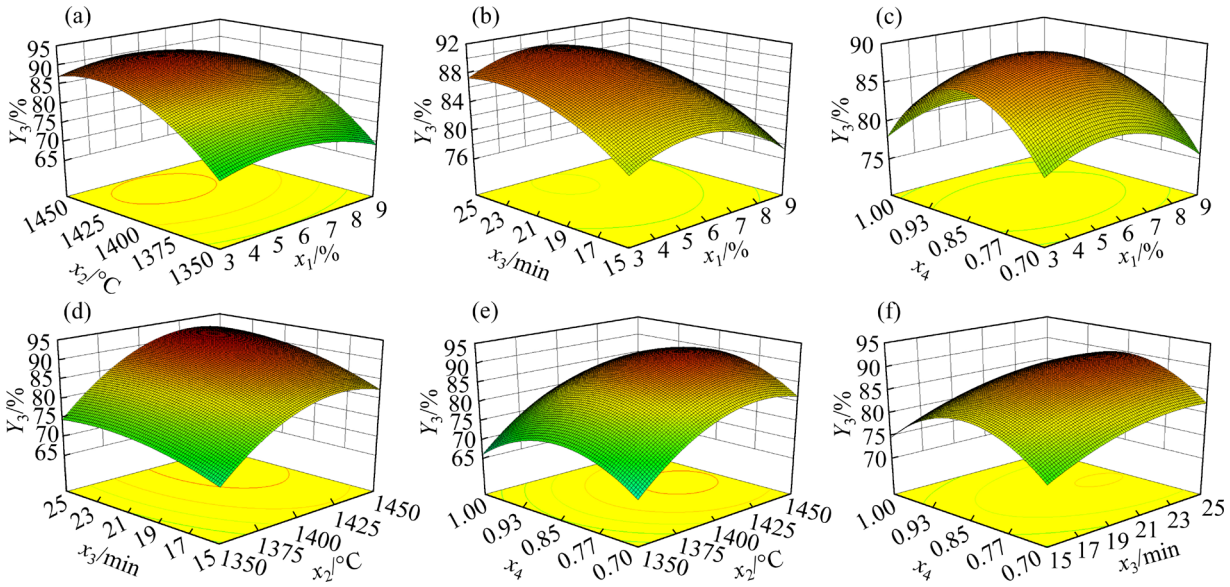

Fig. 7 3D response surface of effects of laterite nickel ore addition (x_1), reduction temperature (x_2), reduction time (x_3) and FC/O (x_4) on Ni recovery (Y_3)

Table 7 Scope of specific optimization constraints

Parameter	Goal	Lower limit	Upper limit	Importance
Laterite nickel ore addition (x_1)/%	Is in range	3.00	9.00	3
Reduction temperature (x_2)/°C	Is in range	1350.00	1450.00	3
Reduction time (x_3)/min	Is in range	15.00	25.00	3
FC/O (x_4)	Is in range	0.70	1.00	3
Fe recovery (Y_1)/%	Maximize	51.73	100.00	3
Cr recovery (Y_2)/%	Maximize	43.18	100.00	3
Ni recovery (Y_3)/%	Maximize	53.96	100.00	3

the predicted results from the model are the Fe recovery of 93.15%, Cr recovery of 91.63%, and Ni recovery of 92.70%.

The CBSL reduction experiment was conducted under the optimum conditions, and the results are shown in Table 8. The experimental results for Fe, Cr and Ni recovery are 92.36%, 90.67% and 93.64%, respectively, which are similar to the predicted results, and the errors are 0.85%, 1.05% and 1.02%, respectively. The multiobjective optimization process for the parameters reveals the sufficient accuracy and reliability of the results predicted by the model. The recovery rate of the Ni reached 93.64%, achieving the efficient recovery of this metal oxide in stainless steel dust, especially for the recovery of Ni with a high price.

Table 8 Predicted and experimental results under optimal conditions

Parameter	Predicted result	Experimental result	Error/%
Laterite nickel ore addition (x_1)/%	5.47	5.47	0.00
Reduction temperature (x_2)/°C	1428.02	1428.00	0.0014
Reduction time (x_3)/min	23.10	23.00	0.43
FC/O (x_4)	0.85	0.85	0.00
Fe recovery (Y_1)/%	93.15	92.36	0.85
Cr recovery (Y_2)/%	91.63	90.67	1.05
Ni recovery (Y_3)/%	92.70	93.64	1.02

3.7 Optimization product analysis

The reduction products obtained under the optimized conditions were screened to obtain Fe−Cr−Ni−C alloy particles and self-powdered slag. The macromorphology is shown in Fig. 8. Figure 8 shows that the reduced metal particles are large and cooled and separated from the slag. The addition of laterite nickel ore reduces the basicity of raw materials and improves the recovery of metal and the degree of pulverization and separation of slag. Under the optimized conditions, the recovery rates of metal Fe, Cr and Ni of stainless steel dust reduction products are 92.36%, 90.67% and 93.64%, respectively. The grades of Fe, Cr and Ni in Fe−Cr−Ni−C alloy particles are 62.33%, 18.76% and 4.61%, respectively, and the contents of harmful elements P and S are very low at 0.0090% and 0.013%, respectively. The Fe−Cr−Ni−C alloy particles obtained by recovering the solid waste stainless steel dust produced by smelting stainless steel have a high metal grade and low content of harmful components. The reduced product consisting of Fe−Cr−Ni−C alloy particles can be directly used as excellent steelmaking raw materials in the steelmaking process, to adjust the liquid steel composition in the stainless steel smelting process, and obtain the stainless steel products.

The XRD phase analysis of the reduced product slag is shown in Fig. 9. The main phases in the reduction product slag are Ca_2SiO_4, $Ca_3Mg(SiO_4)_2$, SiO_2 and MgO. Ca_2SiO_4 expands in volume during cooling, which may promote the separation of reduction product slag and metal particles, and the slag composition has also reached good conditions. Under the optimized conditions, the recovery rates of Fe, Cr and Ni reach more than 90%. This study has important guiding significance for the effective recycling of secondary iron containing solid wastes such as stainless steel dust.

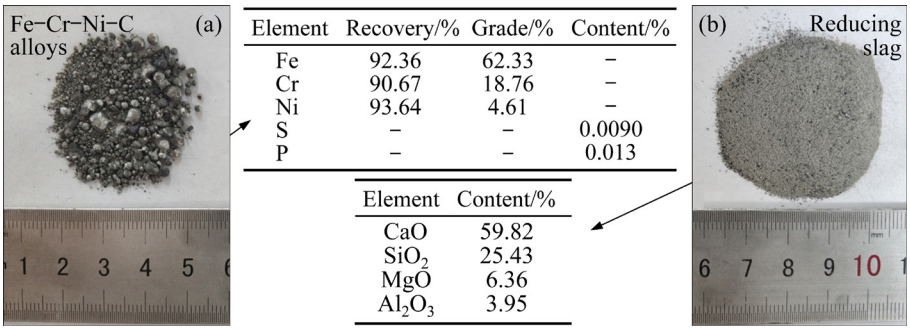

Element	Recovery/%	Grade/%	Content/%
Fe	92.36	62.33	−
Cr	90.67	18.76	−
Ni	93.64	4.61	−
S	−	−	0.0090
P	−	−	0.013

Element	Content/%
CaO	59.82
SiO_2	25.43
MgO	6.36
Al_2O_3	3.95

Fig. 8 Analysis of CBSL reduction products under optimized conditions

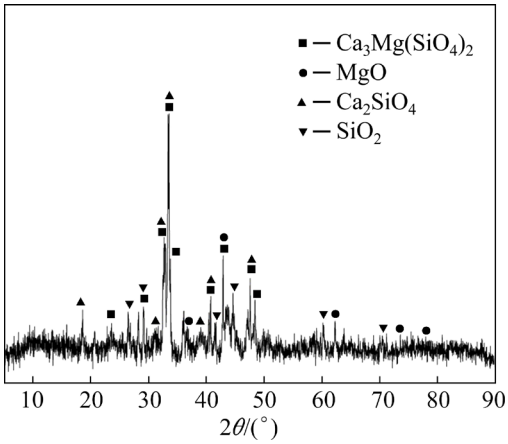

Fig. 9 XRD pattern of reduced slag

4 Conclusions

(1) Quadratic models of Fe, Cr and Ni recovery from CBSL reduction products were successfully established using RSM. The significant parameters influencing the quadratic models were determined using ANOVA, and the accuracy of the models was verified.

(2) Significant interactions between the amount of laterite nickel ore added and reduction temperature, the amount of laterite nickel ore added and reduction time, and the reduction temperature and reduction time are observed. The interactions between the amount of added laterite nickel ore and FC/O, reduction temperature and FC/O, and reduction time and FC/O are low. The influence order of each parameter on the recovery of Fe, Cr and Ni is as follows: reduction temperature > reduction time > amount of laterite nickel ore added > FC/O.

(3) Through the multiobjective collaborative optimization of the response surface method, the final optimization parameters are 5.47% of added laterite nickel ore, a reduction temperature of 1428.02 °C, reduction time of 23.10 min, and FC/O of 0.85. The model predicts that the Fe, Cr and Ni recovery will be 93.15%, 91.63% and 92.70%, respectively. The experimental results are close to the predicted values, which prove that the model has high accuracy and reliability.

Acknowledgments

The authors are especially grateful to the National Natural Science Foundation of China (No. 51974077), and Xingliao Talent Plan, China (No. XLYC1902118), and special thanks are due to the instrumental analysis from Analytical and Testing Center, Northeastern University, China.

References

[1] SPOOREN J, BINNEMANS K, BJÖRKMALM J, BREEMERSCH K, DAMS Y, FOLENS K, GONZÁLEZ-MOYA M, HORCKMANS L, KOMNITSAS K, KURYLAK W, LOPEZ M, MÄKINEN J, ONISEI S, OORTS K, PEYS A, PIETEK G, PONTIKES Y, SNELLINGS R, TRIPIANA M, VARIA J, WILLQUIST K, YURRAMENDI L, KINNUNEN P. Near-zero-waste processing of low-grade, complex primary ores and secondary raw materials in Europe: Technology development trends [J]. Resources, Conservation and Recycling, 2020, 160: 104919.

[2] LI Xiao-ming, XIE Geng, HOJAMBERDIEV M, CUI Ya-ru, ZHAO Jun-xue. Characterization and recycling of nickel- and chromium-contained pickling sludge generated in production of stainless steel [J]. Journal of Central South University, 2014, 21(8): 3241−3246.

[3] ZHANG Hui-ning, HUI Li, DONG Jian-hong, XIONG Hui-hui. Optimization of the stainless steel dust briquette reduction process for iron, chromium, and nickel recovery [J]. High Temperature Materials and Processes, 2018, 37(8): 785−791.

[4] ZHANG Huai-wei, HONG Xin. An overview for the utilization of wastes from stainless steel industries [J]. Resources, Conservation and Recycling, 2011, 55(8): 745−754.

[5] SHEN Hui-ting, FORSSBERG E, NORDSTRÖM U. Physicochemical and mineralogical properties of stainless steel slags oriented to metal recovery [J]. Resources, Conservation and Recycling, 2004, 40(3): 245−271.

[6] HABIB A, BHATTI H N, IQBAL M. Metallurgical processing strategies for metals recovery from industrial slags [J]. Zeitschrift Für Physikalische Chemie, 2020, 234(2): 201−231.

[7] KIM G, SOHN I. Selective metal cation concentration during the solidification of stainless steel EAF dust and slag mixtures from high temperatures for increased Cr recovery [J]. Journal of Hazardous Materials, 2018, 359(5): 174−185.

[8] JUNG S S, KIM G B, SOHN I. Understanding the solidification of stainless steel slag and dust mixtures [J]. Journal of the American Ceramic Society, 2017, 100(8): 3771−3783.

[9] LIU Pei-jun, LIU Zheng-gen, CHU Man-sheng, TANG-Jue, GAO Li-hua, YAN Rui-jun. Green and efficient utilization of stainless steel dust by direct reduction and self-pulverization [J]. Journal of Hazardous Materials, 2021, 413: 125403.

[10] RI S C, CHU Man-sheng, CHEN Shuang-yin, LIU Zheng-gen, HONG Hun. Self-reduction mechanism of coal composite stainless steel dust hot briquette [J]. Journal of Iron and Steel Research, International, 2016, 23(4): 314−321.

[11] KASAI A, TOYOTA H, NOZAWA K, KITAYAMA S. Reduction of reducing agent rate in blast furnace operation by carbon composite iron ore hot briquette [J]. ISIJ International, 2011, 51(8): 1333−1335.

[12] RI S C, CHU Man-sheng. Separation of metal nugget from self-reduced product of coal composite stainless steel dust briquette [J]. ISIJ International, 2015, 55(8): 1565−1572.

[13] YU Zhi-gang, XIAO Jing-wu, LENG Hai-yan, CHOU Kuo-chih. Direct carbothermic reduction of ilmenite concentrates by adding high dosage of Na_2CO_3 in microwave field [J]. Transactions of Nonferrous Metals Society of China, 2021, 31(6): 1818−1827.

[14] PENG Ji, PENG Bing, YU Di, TANG Mo-tang, SONG Hai-chen, LOBEL J, KOZINSKI J A. Kinetics of isothermal reduction of stainless steelmaking dust pellets [J]. Transactions of Nonferrous Metals Society of China, 2004, 14(3): 593−598.

[15] TANG En, LIANG Xue-zheng, LI Ju-yan, ZHOU Qiang. Research on the process of iron-bearing dust's self-reduction to produce iron nuggets [J]. Advanced Materials Research, 2013, 746: 505−510.

[16] ALBERTSSON G J, TENG L, BJÖRKMAN B. Effect of basicity on chromium partition in CaO−MgO−SiO_2−Cr_2O_3 synthetic slag at 1873 K [J]. Mineral Processing and Extractive Metallurgy, 2014, 123(2): 116−122.

[17] CABRERA-REAL H, ROMERO-SERRANO A, ZEIFERT B, HERNANDEZ-RAMIREZ A, HALLEN-LOPEZ M, CRUZ-RAMIREZ A. Effect of MgO and CaO/SiO_2 on the immobilization of chromium in synthetic slags [J]. Journal of Material Cycles and Waste Management, 2012, 14(4): 317−324.

[18] WU Xing-rong, DONG Xiao-min, WANG Run-tao, LU Hui-hong, CAO Fa-bin, SHEN Xing-mei. Crystallization behaviour of chromium in stainless steel slag: Effect of FeO and basicity [J]. Journal of Residuals Science and Technology, 2016, 13(S1): S57−S62.

[19] ZENG Xian-lai, XU Ming, LI Jin-hui. Examining the sustainability of China's nickel supply: 1950—2050 [J]. Resources, Conservation and Recycling, 2018, 139: 188−193.

[20] ILYAS S, SRIVASTAVA R R, KIM H, ILYAS N, SATTAR R. Extraction of nickel and cobalt from a laterite ore using the carbothermic reduction roasting-ammoniacal leaching process [J]. Separation and Purification Technology, 2020, 232: 115971.

[21] SHIAU J S. Carbothermic reduction of low-grade laterite-graphite composite pellets [J]. Metallurgical Research & Technology, 2020, 117(3): 306.

[22] YUAN Shuai, ZHOU Wen-tao, LI Yan-jun, HAN Yue-xin. Efficient enrichment of nickel and iron in laterite nickel ore by deep reduction and magnetic separation [J]. Transactions of Nonferrous Metals Society of China, 2020, 30(3): 812−822.

[23] KWAK J S. Application of Taguchi and response surface methodologies for geometric error in surface grinding process [J]. International Journal of Machine Tools and Manufacture, 2005, 45(3): 327−334.

[24] AHMADI A, REZAEI M, SADEGHIEH S M. Interaction effects of flotation reagents for SAG mill reject of copper sulphide ore using response surface methodology [J]. Transactions of Nonferrous Metals Society of China, 2021, 31(3): 792−806.

[25] GHASEMI S, FARHADIZADEH A R, GHOMI H. Effect of frequency and pulse-on time of high power impulse magnetron sputtering on deposition rate and morphology of titanium nitride using response surface methodology [J]. Transactions of Nonferrous Metals Society of China, 2019, 29(12): 2577−2590.

[26] BEZERRA M, SANTELLI R E, OLIVEIRA E P, VILLAR L S, ESCALEIRA L A. Response surface methodology (RSM) as a tool for optimization in analytical chemistry [J]. Talanta, 2008, 76(5): 965−977.

[27] SHAHNAZI A, FIROOZI S, FATMEHSARI D H. Selective leaching of arsenic from copper converter flue dust by Na_2S and its stabilization with $Fe_2(SO_4)_3$ [J]. Transactions of Nonferrous Metals Society of China, 2020, 30(6): 1674−1686.

[28] LIU Pei-jun, LIU Zheng-gen, CHU Man-sheng, YAN Rui-jun, LI Feng, TANG Jue. Effect of basicity on direct reduction and self-pulverization of stainless steel dust [J]. Journal of Sustainable Metallurgy, 2022, 8(1): 430−442.

[29] IBORRA-BERNAD C, GARCÍA-SEGOVIA P, MARTÍNEZ-MONZÓ J. Effect of vacuum cooking treatment on physicochemical and structural characteristics of purple-flesh potato [J]. International Journal of Food Science & Technology, 2014, 49(4): 943−951.

[30] NADIROV R K, SYZDYKOVA L I, ZHUSSUPOVA A K, USSERBAEV M T. Recovery of value metals from copper smelter slag by ammonium chloride treatment [J]. International Journal of Mineral Processing, 2013, 124(22): 145−149.

[31] ZHANG Bei-kai, GUO Xue-yi, WANG Qin-meng, TIAN

Qing-hua. Thermodynamic analysis and process optimization of zinc and lead recovery from copper smelting slag with chlorination roasting [J]. Transactions of Nonferrous Metals Society of China, 2021, 31(12): 3905−3917.

[32] SIMATE G S, NDLOVU S, GERICKE M. Bacterial leaching of nickel laterites using chemolithotrophic microorganisms: Process optimization using response surface methodology and central composite rotatable design [J]. Hydrometallurgy, 2009, 98(3/4): 241−246.

[33] LIANG Guo-bin, TANG Jiang-hong, LIU Wei-ping, ZHOU Quan-fa. Optimizing mixed culture of two acidophiles to improve copper recovery from printed circuit boards (PCBs) [J]. Journal of Hazardous Materials, 2013, 250/251(15): 238−245.

[34] SHARMA S, MALIK A, SATYA S. Application of response surface methodology (RSM) for optimization of nutrient supplementation for Cr (VI) removal by *Aspergillus lentulus* AML05 [J]. Journal of Hazardous Materials, 2009, 164(2/3): 1198−1204.

[35] WANG Hong-tao, ZHAO Wei, CHU Man-sheng, LIU Zheng-gen, TANG Jue, YING Zi-wei, Effects of coal and iron ore blending on metallurgical properties of iron coke hot briquette [J]. Powder Technology, 2018, 328: 318−328.

[36] DANH L T, MAMMUCARI R, TRUONG P, FOSTER N. Response surface method applied to supercritical carbon dioxide extraction of *Vetiveria zizanioides* essential oil [J]. Chemical Engineering Journal, 2009, 155(3): 617−626.

[37] GUO Xue-yi, LI Dong, WU Zhan, TIAN Qing-hua. Application of response surface methodology in optimizaing the sulfation-roasting-leaching process of nickel laterite [J]. International Journal of Minerals, Metallurgy, and Materials, 2012, 19(3): 199−204.

[38] DAS A K, MANDAL V, MANDAL S C. Design of experiment approach for the process optimisation of microwave assisted extraction of lupeol from *Ficus racemosa* Leaves using response surface methodology [J]. Phytochemical Analysis, 2013, 24(3): 230−247.

[39] ZHANG Yong, GUO Zhao-hui, HAN Zi-yu, XIAO Xi-yuan. Effects of AlN hydrolysis on fractal geometry characteristics of residue from secondary aluminium dross using response surface methodology [J]. Transactions of Nonferrous Metals Society of China, 2018, 28(12): 2574−2581.

不锈钢粉尘和红土镍矿碳热还原新工艺多目标协同优化

刘培军[1,2,3]，柳政根[1,2,3]，储满生[4]，闫瑞军[1,2,3]，李 峰[1,2,3]，唐 珏[1,2,3]

1. 东北大学 冶金学院，沈阳 110819；
2. 东北大学 低碳钢铁前沿技术研究院，沈阳 110819；
3. 东北大学 辽宁省低碳钢铁前沿技术工程研究中心，沈阳 110819；
4. 东北大学 轧制与连轧自动化国家重点实验室，沈阳 110819

摘 要：采用基于响应面法的中心复合设计，通过碳热还原实现不锈钢粉尘和红土镍矿中 Fe、Cr 和 Ni 金属回收的多目标协同优化，获得高金属回收率和高品位 Fe−Cr−Ni−C 合金颗粒。结果表明，红土镍矿的配入量和还原温度对金属回收率有显著影响，还原产物中金属 Fe、Cr 和 Ni 的回收率之间存在显著的交互作用。通过模型优化得到的最优工艺参数为：红土镍矿配入量 5.47%、还原温度 1428.02 ℃、还原时间 23.10 min 和碳氧比(FC/O)0.85。该模型的 Fe、Cr 和 Ni 的回收率预测结果分别为 93.15%、91.63%和 92.70%。

关键词：不锈钢粉尘；红土镍矿；金属回收；响应面法；Fe−Cr−Ni−C 合金颗粒

(Edited by Xiang-qun LI)